*metals*

*Article*

# Investigation of Surface Integrity of 304 Stainless Steel in Turning Process with Nanofluid Minimum-Quantity Lubrication Using h-BN Nanoparticles

**Min Fu [1,2], Guangchun Xiao [1,2,3,*], Hui Chen [1,2,3], Jingjie Zhang [1,2], Mingdong Yi [1,2], Zhaoqiang Chen [1,2,3] and Chonghai Xu [1,2,3,*]**

[1] School of Mechanical Engineering, Qilu University of Technology (Shandong Academy of Sciences), Jinan 250353, China; 10431210113@stu.qlu.edu.cn (M.F.); chenhui@qlu.edu.cn (H.C.); zjj@qlu.edu.cn (J.Z.); yimingdong@qlu.edu.cn (M.Y.); czq@qlu.edu.cn (Z.C.)
[2] Key Laboratory of Equipments Manufacturing and Intelligent Measurement and Control, China National Light Industry, Qilu University of Technology (Shandong Academy of Sciences), Jinan 250353, China
[3] Shandong Institute of Mechanical Design and Research, Jinan 250031, China
* Correspondence: xgc@qlu.edu.cn (G.X.); xch@qlu.edu.cn (C.X.); Tel./Fax: +86-0531-89631986 (G.X.)

**Abstract:** This paper investigates the influence of the concentration and particle size of h-BN nanoparticles in a nanofluid on the surface integrity of 304 austenitic stainless steel during turning, focusing on the cutting force, friction coefficient, cutting temperature, surface roughness, surface residual stress, work hardening capacity, and 3D surface topography. The results show that, compared to dry cutting, the addition of 3 wt.% h-BN nanofluid can reduce the friction coefficient on the rake face by 38.9%, lower the cutting temperature by 43.5%, decrease the surface roughness by 53.8%, decrease the surface residual stress by 61.6%, and reduce the work hardening degree by 27.5%. Two-dimensional profiles and the 3D surface topography display a more balanced peak–valley distribution. Furthermore, by studying the effect of different h-BN particle sizes in nanofluids on the surface integrity of the machined workpiece, it was found that nanoscale particles have a greater tendency to penetrate the tool–chip interface than submicron particles. Moreover, the h-BN particles in the nanofluid play a "rolling effect" and "microsphere" effect, and the sesame oil will also form a lubricating oil film in the knife-chip contact area, thereby reducing the friction coefficient, reducing the cutting force, and improving the machining surface quality.

**Keywords:** nanofluid; minimum-quantity lubrication; hexagonal boron nitride; surface integrity



**Citation:** Fu, M.; Xiao, G.; Chen, H.; Zhang, J.; Yi, M.; Chen, Z.; Xu, C. Investigation of Surface Integrity of 304 Stainless Steel in Turning Process with Nanofluid Minimum-Quantity Lubrication Using h-BN Nanoparticles. *Metals* **2024**, *14*, 583. https://doi.org/10.3390/met14050583

Academic Editor: Matteo Benedetti

Received: 22 April 2024
Revised: 8 May 2024
Accepted: 13 May 2024
Published: 16 May 2024



## 1. Introduction

The alterations in surface and subsurface performance resulting from mechanical machining play the vital role in the utilization of engineering parts with the necessary shape and size, particularly in fields with high-performance requirements including aerospace, nuclear engineering, and medical applications [1]. During machining processes such as drilling, turning, and milling, a small portion of the heat generated (approximately 8% to 10%) is transferred to the cutting tool, while a majority of the heat is distributed to the chips and the workpiece [2]. Determining the exact distribution of heat is challenging and depends on factors such as the material of the workpiece, the material and geometry of the cutting tool, and the cutting conditions [3]. The surface integrity of austenitic stainless steel is significantly affected by microhardness, work hardening changes, and induced surface residual stresses caused by mechanical machining [4]. Therefore, it is necessary to control cutting heat by changing cutting parameters, selecting appropriate tools, etc. One method to reduce heat and cutting temperatures is by lowering the average friction coefficient in the contact zone between the cutting tool and chips, primarily through the application of liquid or gas media as the coolant and lubricant. Typically, cutting fluid is the direct approach to addressing the issue [5].

In addition to effectively improving the cooling and lubrication capacity of the tool–workpiece interface during machining processes, cutting fluids also help to remove chips from the cutting contact zone [6]. Nevertheless, the utilization of traditional cutting fluids has negative implications for the environment, human health, and production expenses [7]. The chemicals involved have harmful impacts on the natural environment and pose risks to human health upon contact with the skin. In addition, there are challenges related to the storage, supply, and harmless handling of the cutting fluids [8]. For these reasons, researchers have been striving in recent years to reduce the reliance on cutting fluids during the chip evacuation processes [9]. Minimum-quantity lubrication (MQL) is the effective way to address the aforementioned issues.

This method is based on generating micron-sized droplets by atomizing a liquid using compressed air through an air mist nozzle, which is then directly injected into the machining zone. It reduces the use of the cutting fluids and promotes sustainability [10]. The research conducted by Jagdeep Sharma et al. [11] on AISI D12408 steel cutting shows that MQL achieved better results in terms of tool–workpiece interface temperature and surface roughness. An investigation into the cutting of AISI D12408 steel by Jagdeep Sharma et al. [11] revealed that MQL yielded superior outcomes in terms of surface roughness and cutting temperature. This suggests that MQL has the potential to enhance surface integrity. Tazehkand et al. [12] conducted a comparative study investigating the impact of a flood coolant and MQL on the cutting of Inconel 740. This study found that, compared to the use of flood coolant, MQL significantly reduced surface roughness by 41% and cutting edge temperature by 52%.

However, in some cases, the oil mist may not possess sufficient thermal conductivity to effectively influence the cutting contact area. When this occurs, it can lead to inadequate heat dissipation and lubrication, potentially resulting in increased heat generation and friction [13,14]. Therefore, many researchers choose to add nanoparticles to cutting fluids to enhance the lubrication and cooling capabilities of the oil mist [15].

Current research has confirmed that adding solid additives to fluids can significantly enhance the surface integrity of machined components. Shokrani et al. [16] found that adding electrically charged tungsten disulfide ($WS_2$) to cutting fluids can enhance cooling and lubrication during machining, thereby significantly enhancing surface integrity. Makhesana et al. [17] studied the impact of $MoS_2$ and graphite nanofluids on the surface integrity of cutting Inconel 625. They found that the solid lubricants added in NMQL can penetrate the machining interface more effectively.

Among the different kinds of nanoparticles for generating nanofluids, h-BN nanoparticles have also been utilized. The lattice structure of h-BN possesses a unique layered structure, where the bonding between layers is relatively weak, allowing for the formation of sliding layers on the surface. This layered structure enables the surface of hexagonal boron nitride to exhibit relative slip when subjected to stress, thereby reducing friction. Due to this crystal structure, h-BN exhibits good lubricating properties in industrial applications and provides opportunities for reducing friction and wear [18]. Wang et al. [19] added 1–5 wt.% h-BN in castor oil and found that 1 wt.% h-BN nanofluid decreased the wear rate by 51.74%. Kim et al. [20] studied the influence of h-BN-based nanofluids on the micro-milling of TC11 and found that the h-BN-based nanofluid effectively reduced milling forces and improved the surface quality. Talib et al. [21] studied the effect of adding 0.05–0.5 wt.% h-BN nanofluids, and observed that 0.05 wt.% h-BN nanofluid resulted in improved tribological performance, enhanced machining efficiency, and better surface quality. However, the aforementioned study did not consider the influence of different h-BN nanofluid concentrations and particle sizes on machining surface integrity.

The main objective of this study is to evaluate the influence of h-BN-NMQL on the surface integrity of 304 stainless steel during the turning process. Nano-sized h-BN particles were chosen as the solid additive in the experiments, and sesame oil was selected as the base oil. Additionally, to further investigate the impact of h-BN nanoparticles in the nanofluid on

the surface integrity of the workpiece during the turning process of 304 stainless steel, this study also included cutting experiments with h-BN-NMQL utilizing different particle sizes.

## 2. Materials and Methods

### *2.1. Workpiece Materials and Ceramic Tools*

The chemical composition of the 304 stainless steel used in this experiment is listed in Table 1.

**Table 1.** The chemical content of the workpiece (wt.%).

| C | Mn | P | Si | Cr | Ni | Fe |
|---|---|---|---|---|---|---|
| ≤0.08 | ≤2 | ≤0.045 | ≤1.0 | 18–20 | 8–11 | balance |

The ceramic tool was $Al_2O_3$/Ti(C,N) (Dezhou Rock High Performance Ceramics Co. Ltd., Dezhou, China). Its mechanical properties are shown in Table 2. The ISO standard code is SNGN120408 [22]. The dimensions of the tool are 12.7 mm × 12.7 mm × 4.76 mm. The tool holder model is Kenner CSSNR 252525 M12–MN7 (Kennametal Inc., Pittsburgh, PA, USA). The cutting tool was mounted on the holder, forming the following geometrical shapes: flank angle $\alpha_0$: 5°; rake angle $\gamma_0$: −5°; and the principal angle $\kappa_r$: 45°.

**Table 2.** Mechanical properties of ceramic tools.

| Tool Material | Density ($g/cm^3$) | Flexural Strength (MPa) | Fracture Toughness ($MPa \cdot m^{1/2}$) | Hardness (GPa) |
|---|---|---|---|---|
| $Al_2O_3$/Ti(C,N) | 4.40 | 650 | 5.5 | 20 |

### *2.2. Preparation of Nanofluids*

In this experiment, nano-h-BN particles (purity: 99.9%; particle size: 20 nm; Shanghai CW-Nano Science & Technology Co., Ltd., Shanghai, China) were used. Additionally, to investigate the influence of particle sizes on the surface integrity, the particle size of the h-BN nanofluid was determined using four different particle sizes: 20 nm, 40 nm, 80 nm, and 500 nm.

Shanghai Yuanye Bio-Technology Co., Ltd., Shanghai, China provided the refined sesame oil as the base oil, while refined olive oil from the same source was used as the reference oil.

Figure 1 shows the XRD and TEM images of the nano-h-BN, along with the preparation method of the h-BN nanofluid. The preparation process primarily involves a two-step procedure. Initially, the nano-h-BN is carefully weighed using an analytical balance. Subsequently, it is mixed with sesame oil for 30 min utilizing a mechanical stirrer. Following this, the mixture is treated in a 50 kHz frequency, 800 W power ultrasonic water bath for 60 min. This step aims to prevent the aggregation of the nano-h-BN in the base oil and achieve a uniform dispersion.

### *2.3. Experimental Design and Measuring Equipment*

The viscosity of the fluids was recorded using a rheometer (MCR302, Anton Paar, Graz, Austria) at temperatures of 25 °C, 40 °C, 60 °C, and 80 °C. After that, the ellipse method was used to measure the contact angle, and its measurement principle is shown in Figure 2. The contact angle measuring instrument SZ-CAMB3 produced by Shanghai Xuanjun Company (Shanghai, China) was used to measure the contact angle. The experiment was carried out at room temperature of 25 °C, and the liquid was measured several times. Polished 304 austenitic stainless steel was used as the base solid in the experiment.

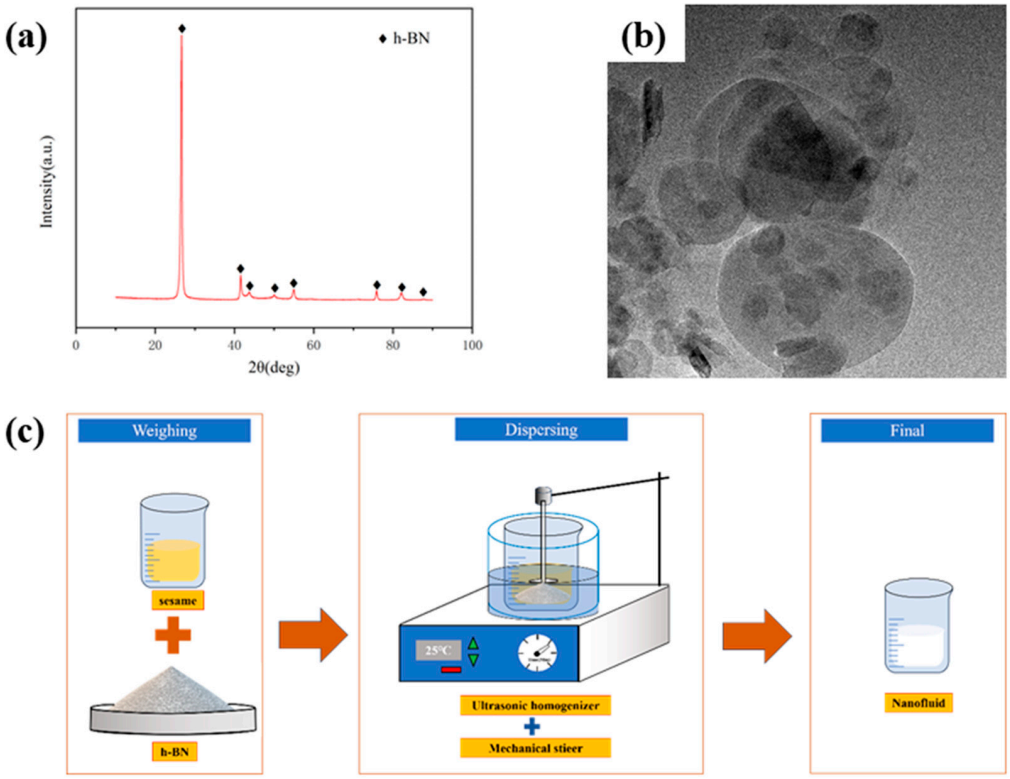


**Figure 1.** Characteristics and production of h-BN nanofluids: (**a**) XRD of h-BN particles, (**b**) TEM of h-BN particles, (**c**) scheme for producing h-BN nanofluids.

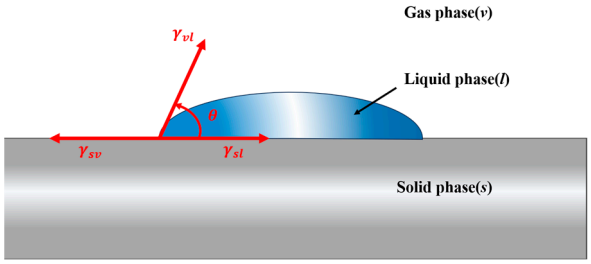


**Figure 2.** Measurement principle of droplet contact angle.

Figure 3 shows the experimental setup. This study used a standard horizontal machine CDE6140A, and the MQL equipment employed the LXZS micro-injection device produced by Wuxi Longxi Company (Wuxi, China), as depicted in Figure 3a. The cutting fluid flow rate was 60 mL/h. The air pressure was 0.4 MPa. The spray angle between the nozzle and the rake face was 30°. The nozzle standoff distance was 30 mm. Temperature data were measured by an infrared thermometer (FLIR 315A, FLIR, Wilsonville, OR, USA). The cutting force was measured by a dynamometer (Kistler 9129 AA, Kistler, Sindelfingen, Germany).

The surface roughness was measured by a roughness tester (TR 240, TIME, Beijing, China). The 304 stainless-steel workpiece was then cut into 5 mm × 5 mm × 5 mm blocks using the wire cutting method to obtain surface samples. After deburring, degreasing, cleaning, and ultrasonic cleaning processes, the 2D and 3D surface morphologies of the processed workpiece were observed using a three-dimensional light microscope (Contour Elite K, Bruker, Bremen, Germany). The microhardness was measured by a microhardness tester (HXD-1000TMC, Tai Ming, Shanghai, China) to determine the degree of work hardening. The experimental load was set to 200 kgf and the load holding time was 10 s. To reduce measurements errors, three microhardness measurements were taken at different positions on the same surface, and the average value was obtained as the microhardness value of the parameter. To avoid the impact of unevenness on the machined surface of the samples,

the first measurement point for microhardness was taken at a distance of 50 µm from the workpiece surface, and subsequent measurements were taken every 50 µm until three consecutive microhardness values close to the base material hardness were obtained. The surface residual stress measurement instrument used was the XSTRESS3000 portable X-ray stress analyzer provided by Beijing Huaou Century Photoelectric Technology Co., Ltd., Beijing, China, which was used to test the surface residual stress. The specific experimental test equipment is shown in Figure 4.

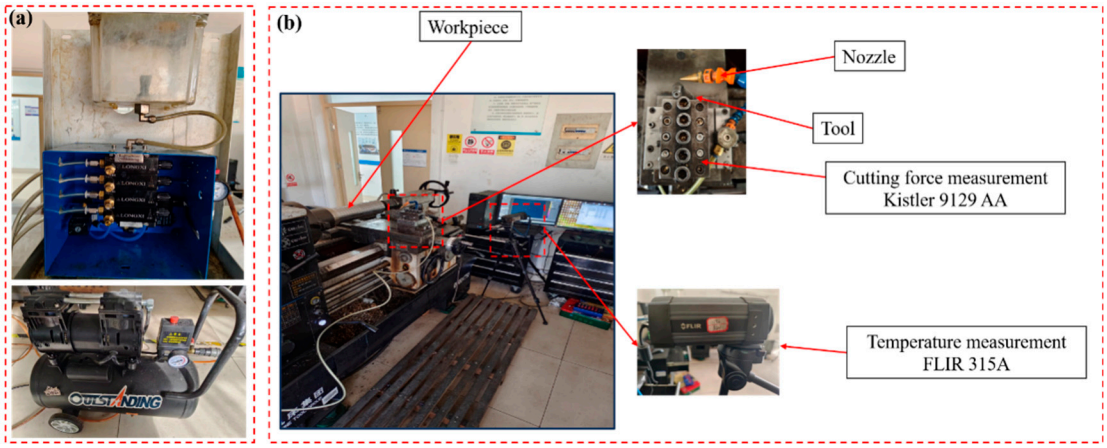


**Figure 3.** Experimental setup for turning tests: (**a**) MQL equipment, (**b**) cutting experimental equipment.

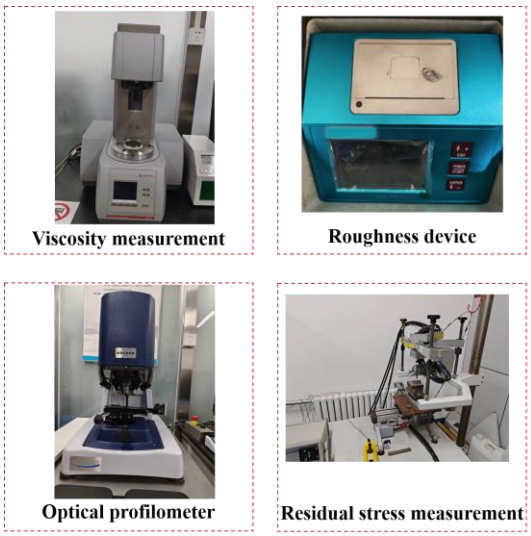


**Figure 4.** Experimental test equipment.

The experiment on h-BN nanofluid concentration was conducted in six different cutting environments, dry, sesame oil, sesame oil + 0.5 wt.% h-BN, sesame oil + 1 wt.% h-BN, sesame oil + 3 wt.% h-BN, and sesame oil + 5 wt.% h-BN, with experimental contents as shown in Table 3. As shown in Table 4 experiments on the particle size of h-BN nanofluid were carried out using four different particle sizes: 20 nm, 40 nm, 80 nm, and 500 nm. The cutting parameters are consistent with the concentration experiments. To ensure reproducibility, three experiments were conducted in each group.

**Table 3.** Experimental design 1.

| No | Cutting Environment | Nanoparticle Size (h-BN) | Cutting Speed (m/min) | Feed Rate (mm/rev) | Cutting Depth (mm) | Distance (m) |
|---|---|---|---|---|---|---|
| 1 | Dry | None | 186 | 0.102 | 0.3 | 500 |
| 2 | Sesame oil | None | 186 | 0.102 | 0.3 | 500 |
| 3 | Sesame oil + 0.5 wt.% h-BN | 20 nm | 186 | 0.102 | 0.3 | 500 |
| 4 | Sesame oil + 1 wt.% h-BN | 20 nm | 186 | 0.102 | 0.3 | 500 |
| 5 | Sesame oil + 3 wt.% h-BN | 20 nm | 186 | 0.102 | 0.3 | 500 |
| 6 | Sesame oil + 5 wt.% h-BN | 20 nm | 186 | 0.102 | 0.3 | 500 |

**Table 4.** Experimental design 2.

| No | Cutting Environment | Nanoparticle Size (h-BN) | Cutting Speed (m/min) | Feed Rate (mm/rev) | Cutting Depth (mm) | Distance (m) |
|---|---|---|---|---|---|---|
| 1 | Dry | None | 186 | 0.102 | 0.3 | 500 |
| 2 | MQL | None | 186 | 0.102 | 0.3 | 500 |
| 3 | NMQL | 20 nm | 186 | 0.102 | 0.3 | 500 |
| 4 | NMQL | 40 nm | 186 | 0.102 | 0.3 | 500 |
| 5 | NMQL | 80 nm | 186 | 0.102 | 0.3 | 500 |
| 6 | NMQL | 500 nm | 186 | 0.102 | 0.3 | 500 |

## 3. Results and Discussion

### *3.1. Influence of Nano-h-BN Content on the Surface Integrity of 304 Stainless Steel*

#### 3.1.1. Physical Characterization of the Fluids

Figure 5 shows the viscosity of different kinds of fluids at 25 °C, 40 °C, 60 °C, and 80 °C. As depicted in Figure 5, the viscosity rises in correlation with the increase in h-BN mass fraction, owing to the combined effects of Brownian motion of h-BN nanoparticles, the impact of surrounding liquid molecules, and van der Waals forces. The addition of h-BN brings about an increased concentration of nanoparticles per unit volume. Consequently, this raises the internal frictional resistance and modifies the shear force within the suspension, ultimately resulting in a heightened viscosity [23]. In addition, due to the high surface energy of h-BN nanoparticles, the increasing number of aggregated particles also increases the energy needed to overcome internal friction, leading to an increase in viscosity.

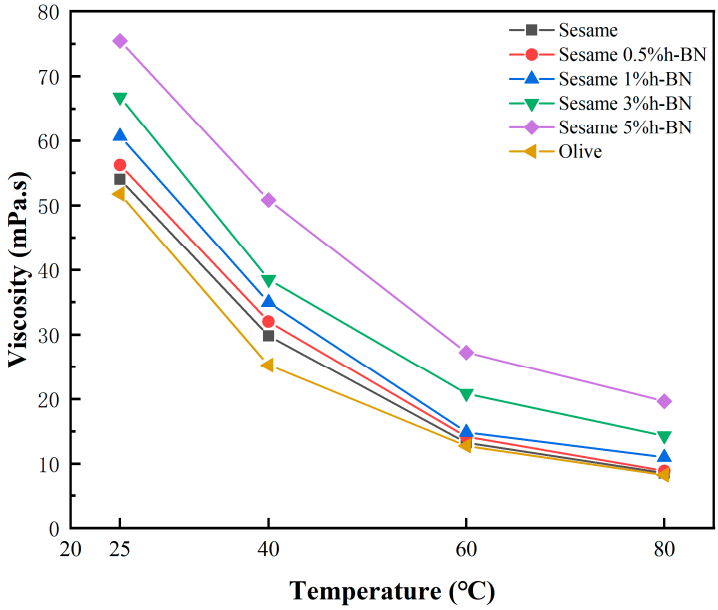


**Figure 5.** The viscosity–temperature curve of different kinds of nanofluids.

The viscosity of the sesame oil with 5 wt.% h-BN of 80 °C is 128.8% higher compared to pure sesame oil. Furthermore, the viscosity–temperature relationship indicates that the pronounced random motion of h-BN nanoparticles substantially slows the viscosity reduction of sesame oil at elevated temperatures. This phenomenon contributes to the improvement in fluid-lubricating film stability. This is mainly because the temperature increase in the h-BN nanofluid weakens the adhesion effects between particles and molecules, thereby reducing the viscosity of the h-BN nanofluid.

Figure 6 illustrates the contact angle (θ) of the nanofluid. A reduced contact angle signifies an increased wetting area of the mist droplets. This enhanced wetting capability facilitates the fluid's penetration through the capillary flow [24]. Based on the observation of Figure 6, the contact angles of olive oil and sesame oil are recorded as 34.245° and 18.346°, respectively. The contact angle of olive oil exhibits an increase of 86.7% in comparison to sesame oil. As previously discussed, a higher contact angle suggests reduced fluidity and diminished heat transfer efficiency, so the wetting properties of olive oil will have a substantial impact. Consequently, in this experiment, sesame oil is selected. Figure 6c–f reveal a decrease in contact angle from 17.553° to 11.640° as the h-BN content increases. A larger wetted area facilitates the coverage of more lubrication regions, thereby enhancing effective lubrication. The decline in contact angle leads to a larger wetting area and ensures ample lubrication [15].

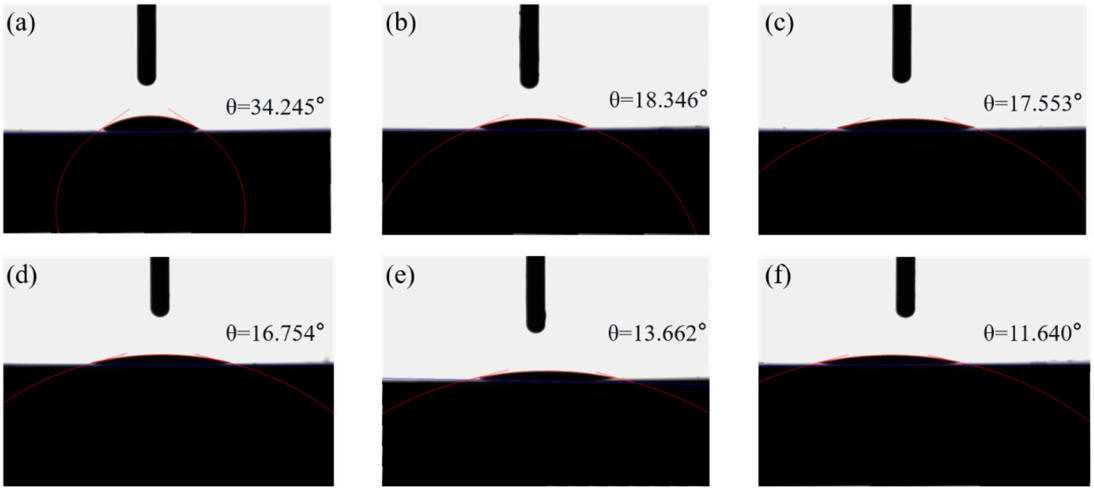


**Figure 6.** The contact angles (θ) of different kinds of cutting fluids on the 304 stainless steel are as follows: (**a**) olive oil, (**b**) sesame oil, (**c**) sesame oil with 0.5 wt.% h-BN, (**d**) sesame oil with 1 wt.% h-BN, (**e**) sesame oil with 3 wt.% h-BN, and (**f**) sesame oil with 5 wt.% h-BN.

#### 3.1.2. Cutting Force and Coefficient of Friction

Figure 7 shows the coefficient of friction of the tool rake face and cutting force. The average coefficient of friction ($\mu$) can be determined by employing Equation (1) [25]:

$$\mu = \tan\left(\gamma_0 + arctan\frac{F_P}{F_C}\right) \quad (1)$$

where $\gamma_0$ is the tool rake angle, $F_p$ is the radial force, and $F_c$ is the tangential force.

As shown in Figure 7, the results clearly indicate that incorporating h-BN nanofluid at different concentrations leads to a substantial decrease in the friction coefficient. At the mass fraction of 3 wt.% for h-BN, the average friction coefficient reaches its minimum at 0.586. This value is 38.9% smaller than that of dry cutting (0.814) and 17.5% lower than that of pure sesame oil (0.693). These results indicate that the inclusion of h-BN particles successfully reduces friction within the tool–chip contact area.

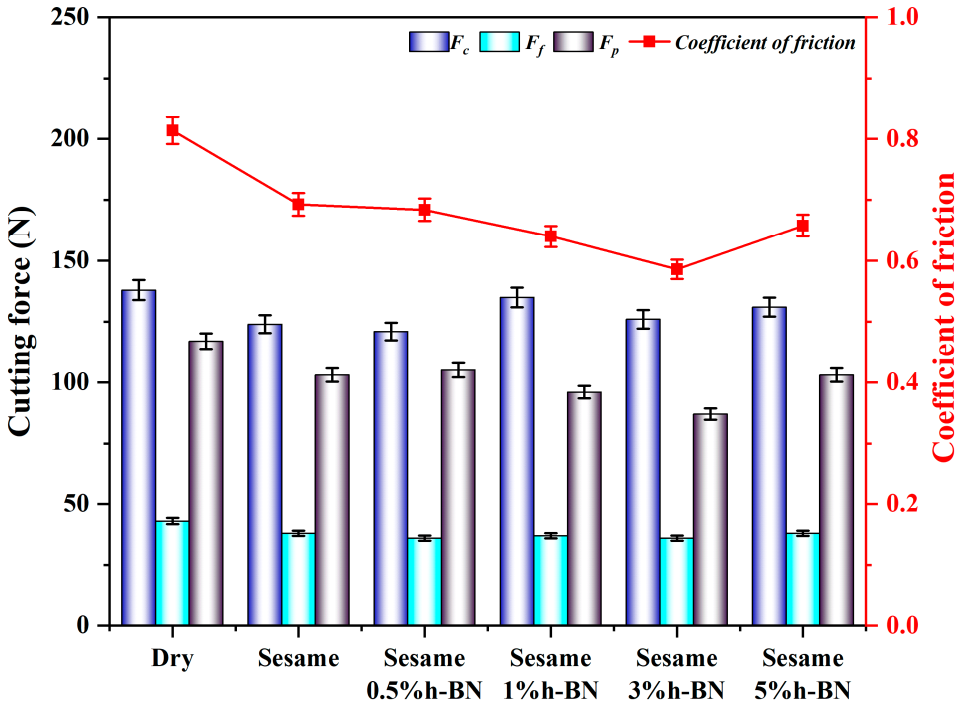


**Figure 7.** Friction coefficient and cutting force in concentration experiment.

When the h-BN particle concentration is too low or too high, there is an increase in average friction coefficient, and each has a main reason. Firstly, at low concentrations, the h-BN particles in the nanofluid may not exhibit the full "microsphere effect" [26]. This effect refers to the ability of the spherical h-BN particles to form a lubricating film, reducing friction. When the concentration is too low, the desired microsphere effect may not be fully realized, leading to higher friction coefficients. Secondly, when the h-BN concentration is too high, an excessive amount of h-BN can cause particle agglomeration and aggregation within the fluid. The presence of large-sized agglomerated nanoparticles hinders their rapid entrance into the tool–chip contact area, resulting in an increased cutting force and reduced cutting efficiency. Additionally, these nanoparticles lose dynamic stability and accumulate within sesame oil, thereby diminishing the fluid's capacity to form a protective film and subsequently elevating the friction coefficient [27].

The utilization of h-BN nanofluid demonstrates the effective reduction in cutting force founded upon the performance of cutting forces in various lubrication conditions. This reduction can be attributed to the cooling and lubricating properties exhibited by sesame oil and h-BN nanoparticles within the tool–chip contact zone. Figure 6 shows that the friction coefficient, which is the significant factor influencing the cutting force [28], is effectively decreased by the penetration of nanofluid into the interior of metal microcracks in the plastic deformation zone. This reduction in friction coefficient subsequently brings about the decrease in cutting force, facilitating the processes [29].

### 3.1.3. Cutting Temperature and Surface Roughness

Figure 8 shows the fluctuation in cutting temperature in different cutting conditions. The results demonstrate that the addition of h-BN improves the heat transfer efficiency of sesame oil. The addition of 3 wt.% h-BN to sesame oil results in a substantial reduction in cutting temperature compared to dry cutting, achieving a reduction of 43.5%. This significant improvement in heat dissipation can be attributed to the enhanced thermal conductivity and convective heat transfer coefficient facilitated by the inclusion of h-BN nanoparticles. Consequently, this leads to an enhanced heat transfer capability, lower cutting forces, and decreased temperature within the cutting zone. Ultimately, these improvements contribute to enhancing the integrity of the machined surface.

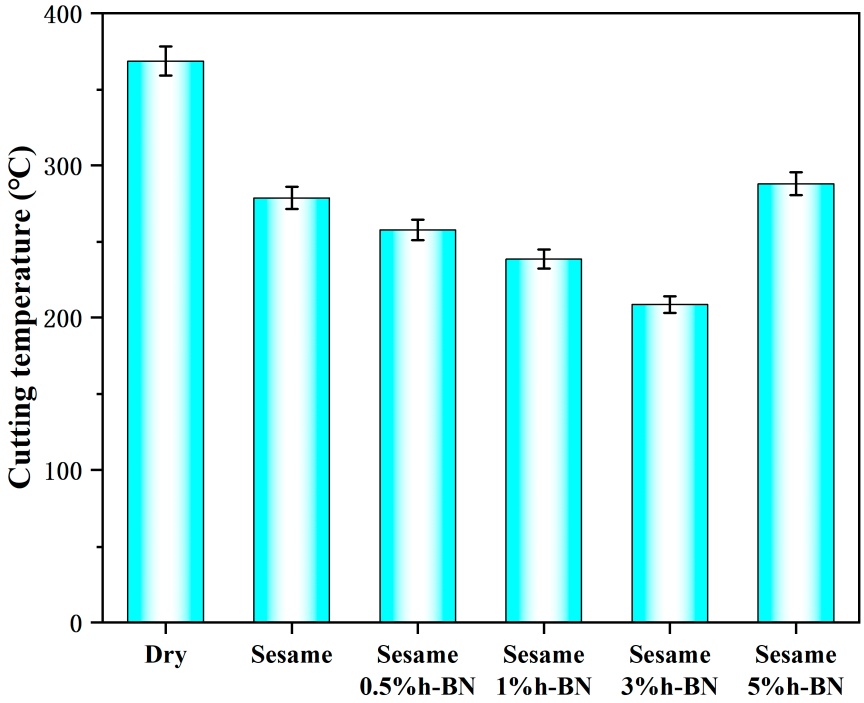


**Figure 8.** Cutting temperature in concentration experiment.

Furthermore, the phenomenon of cutting temperature fluctuations with concentration variation has been explained in the research conducted by Habibnia et al. [30]. When the h-BN content added to sesame oil is low, there are fewer particles actually sprayed into the tool–chip contact area, and a small number of particles cannot exhibit the "microsphere effect". On the contrary, when the h-BN content is too high, excessive amounts of h-BN may lead to particle aggregation in the fluid. In both scenarios, this can cause an increase in friction force in the tool–chip contact area, leading to elevated cutting temperatures, as indicated by the friction coefficient calculation results in Figure 7.

Figure 9 shows the workpiece surface roughness in different cutting conditions. The graph demonstrates that the surface roughness is at its lowest when using sesame oil containing 3 wt.% h-BN. In comparison to dry cutting, the surface roughness decreased by 53.8%. Conversely, the surface roughness of the sesame oil with 5 wt.% h-BN is the most pronounced, exhibiting a 28.7% higher roughness compared to dry cutting. This is because of the excessive accumulation of high-concentration h-BN in the tool–chip contact area during cutting, which hinders the movement of nanoparticles and impairs the lubricating oil film. As a result, friction increases, leading to a continuous deterioration of surface integrity [31]. Previous studies have indicated that h-BN nanofluid functions as a boundary lubricant [21]. Under such lubrication conditions, the integration of h-BN nanoparticles between the tool's rake face and the workpiece surface enhances lubrication by the oil. Simultaneously, the direct interaction of h-BN nanoparticles diminishes the effective contact area between the rake face and the workpiece, thus mitigating the damage inflicted by the rake face on the machined surface.

### 3.1.4. Microhardness Variation and Work Hardening Capacity

Figure 10 shows the microhardness and work-hardening capability of the machined surface in different cutting conditions.

In Figure 10a, the microhardness measurement of the base material is around 210 HV. The surface microhardness varies in different cutting conditions, ranging from 242.1 HV to 299.9 HV. In comparison to the uncut base material, the microhardness of the surfaces increased by 42.8%, 25.8%, 21.8%, 19%, 15.3%, and 20.9%, respectively. The lowest work hardening was achieved with the addition of 3 wt.% h-BN. When the h-BN particle con-

centration is too low or too high, the average friction coefficient increases, bringing about an increase in the work hardening capacity, which is consistent with the variation in cutting temperature. As shown in Figure 10b, the curves exhibit a similar trend across all conditions. The machined surface demonstrates significantly higher hardness than the base material. The hardness values gradually decrease with increasing depth beneath the machined surface, approaching the average value of the workpiece material. The affected zone from machining has a depth of approximately 200 µm due to the plastic deformation during shear deformation, resulting in surface work hardening.

#### 3.1.5. Surface Topography

Figure 11 presents the 3D surface topography images and 2D surface profile in different cutting environments. The images indicate that during dry cutting, the peak-to-valley variances are significantly higher, with the maximum difference between valleys and peaks exceeding 13 µm. When 3 wt.% h-BN sesame oil is added, the maximum difference between valleys and peaks is minimized. In 2D surface profile and 3D surface topography analysis, MQL and NMQL demonstrate a more even distribution of valleys and peaks on the surface. This correlation can be linked to the surface roughness findings discussed in Section 3.1.3.

In the absence of a quick chip evacuation from the cutting zone, especially when machining materials like 304 stainless steel that are prone to chip adhesion and surface scratching, the surface quality deteriorates [32]. Furthermore, the presence of compressed air in the MQL and NMQL systems aids in promptly evacuating chips from the machining zone. The implementation of advanced coolant/lubricants, such as nanofluids, has the potential to decrease the average friction coefficient and effectively eliminate chips from the cutting zone. This outcome subsequently leads to the attainment of a smoother machined surface, which is directly correlated with the friction coefficient findings discussed in Section 3.1.1.

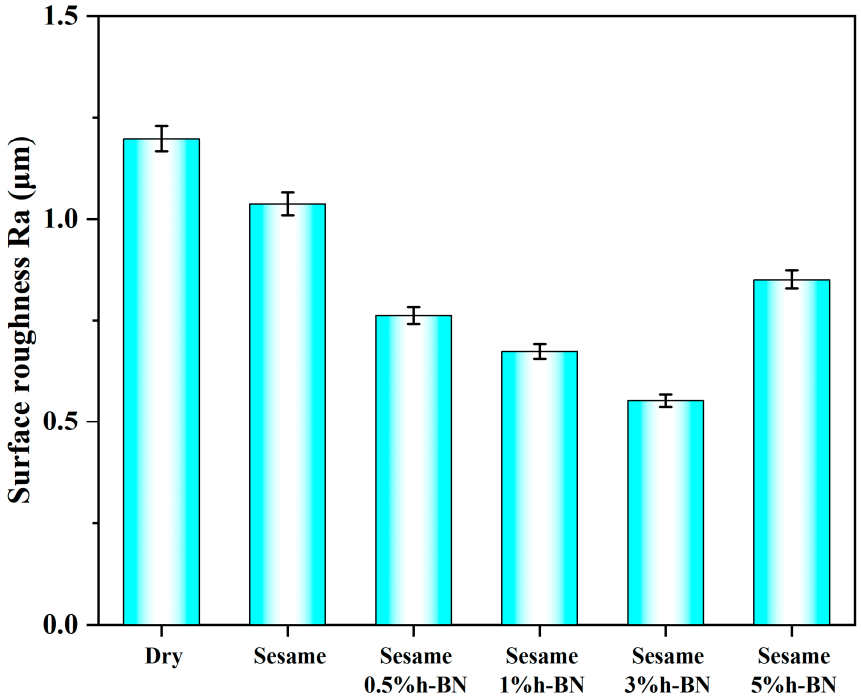


**Figure 9.** Surface roughness in different cutting conditions.

#### 3.1.6. Surface Residual Stress

Figure 12 illustrates the surface residual stress in different cutting conditions. The findings reveal that the residual stresses are predominantly tensile in different cutting conditions, indicating that the thermal effects outweigh the mechanical effects. This can be

attributed to the relatively low thermal conductivity of 304 stainless steel, which causes the heat to accumulate in the cutting region and results in the localized temperature increase [33]. Moreover, the graph depicts that sesame oil with 3 wt.% h-BN demonstrates the lowest surface residual stress. This is attributed to its minimal friction coefficient, thereby reducing the impact of friction forces. This helps reduce surface plastic deformation caused by cutting forces and decreases the generation of residual stress. Moreover, it has the lowest cutting temperature, which is beneficial for reducing the generation of thermal stress and residual stress. Adding 3 wt.% h-BN in sesame oil results in the highest surface quality, and better surface quality helps reduce the generation of residual stress. When the h-BN particle concentration is too low or too high, the average friction coefficient and cutting temperature increase, leading to higher surface residual stresses, which correlate with the friction coefficient results in Section 3.1.1 and Figure 7.

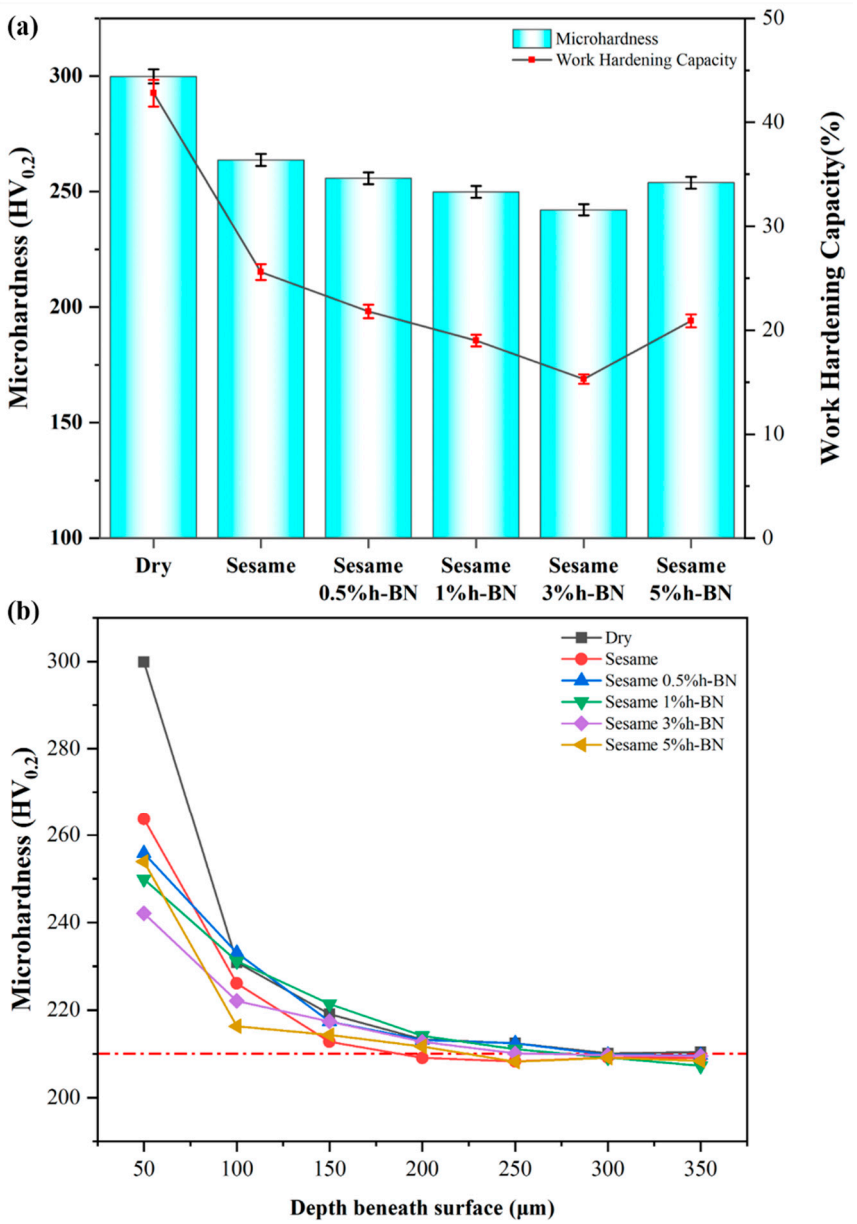


**Figure 10.** Microhardness in different cutting conditions: (**a**) work hardening capacity; (**b**) microhardness of the machined surfaces (the dotted red line represents the microhardness of the substrate).

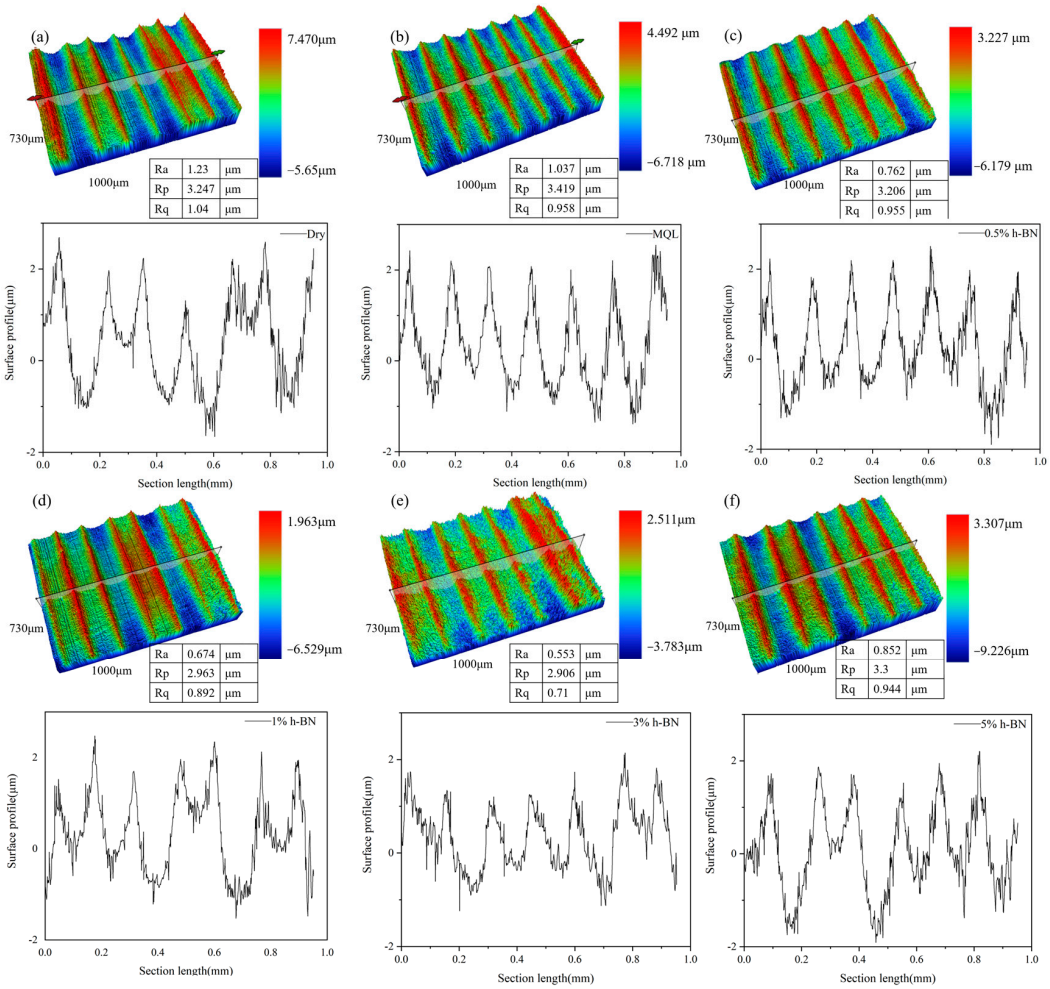


**Figure 11.** The 3D surface topography and 2D surface profile images in different cutting conditions: (**a**) dry, (**b**) sesame oil, (**c**) sesame oil with 0.5 wt.% h-BN, (**d**) sesame oil with 1 wt.% h-BN, (**e**) sesame oil with 3 wt.% h-BN, and (**f**) sesame oil with 5 wt.% h-BN.

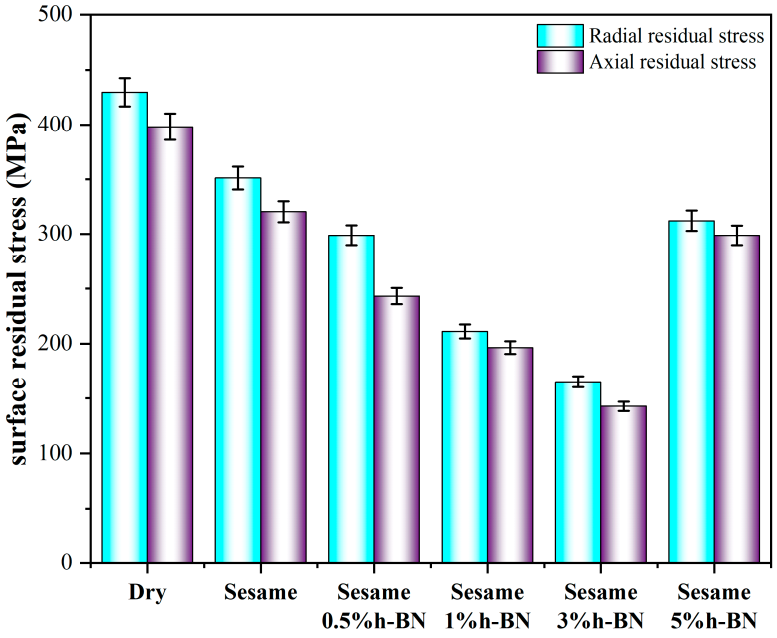


**Figure 12.** Surface residual stress in different cutting conditions.

### *3.2. Effect of h-BN Nanoparticle Size on the Cutting Surface Integrity of 304 Stainless Steel*

Further research on different particle sizes of h-BN in nanofluids is conducted on the surface integrity of 304 stainless steel. Through concentration experiments, the mass fraction of 3 wt.% of h-BN in sesame oil was selected as the base fluid.

#### 3.2.1. Cutting Force and Coefficient of Friction

As per Equation (1), Figure 13 illustrates the variation in the friction coefficient across different h-BN particle sizes. Even under h-BN-NMQL conditions, a considerable reduction in the friction coefficient is evident. In comparison to dry cutting (0.814) and pure sesame oil (0.693), the highest friction coefficient on the rake face is reduced by 38.9% and 15.4%, respectively. Furthermore, minimal disparity in the friction coefficient is observed among the 20 nm, 40 nm, and 80 nm particle sizes under nano-h-BN conditions, ranging from approximately 0.58 to 0.65. However, a notable increase in the friction coefficient to 0.692 is observed when the particle size reaches 500 nm. This suggests that excessively large h-BN particle sizes hinder anti-friction and anti-wear effects of h-BN particles in the tool–chip contact area.

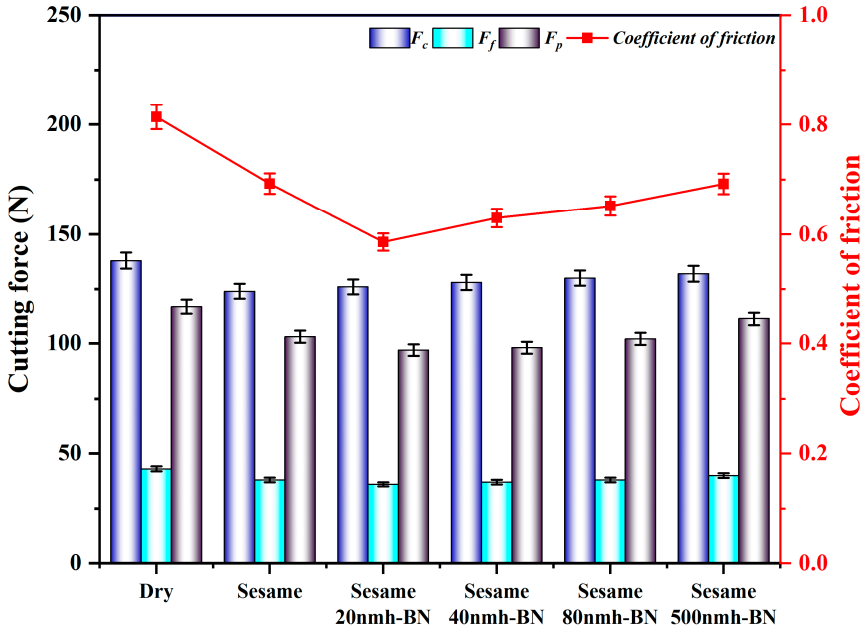


**Figure 13.** Friction coefficients and cutting forces in particle size experiment.

Moreover, the cutting force exhibits a gradual increase with the escalation of h-BN particle size in the nanofluid. Upon reaching a particle size of 500 nm within the submicron range, the cutting force magnitude is observed to approach that of dry cutting, while the friction coefficient also demonstrates relatively poor performance. This situation is disadvantageous for enhancing the surface integrity. Therefore, the particle size experiments indicate that nanoscale h-BN presents superior effects, with a marginal disparity between them and overall improved performance.

#### 3.2.2. Cutting Temperature and Surface Roughness

Figures 14 and 15 display the cutting temperature and surface roughness in the particle size experiments concerning NMQL. Figure 13 demonstrates that the utilization of MQL and NMQL techniques brings about a noteworthy reduction in cutting temperature. In comparison to dry cutting, the maximum reduction in cutting temperature is 35.3%, while the minimum reduction is 23.1%. This indicates that the h-BN nanofluid exhibits stability in reducing cutting temperatures. Moreover, the increase in h-BN particle size from the nanoscale to the submicron scale results in a rise in cutting temperature from 238.7 °C to

283.4 °C. This finding suggests that the particle size of h-BN has an impact on the reduction in cutting temperature.

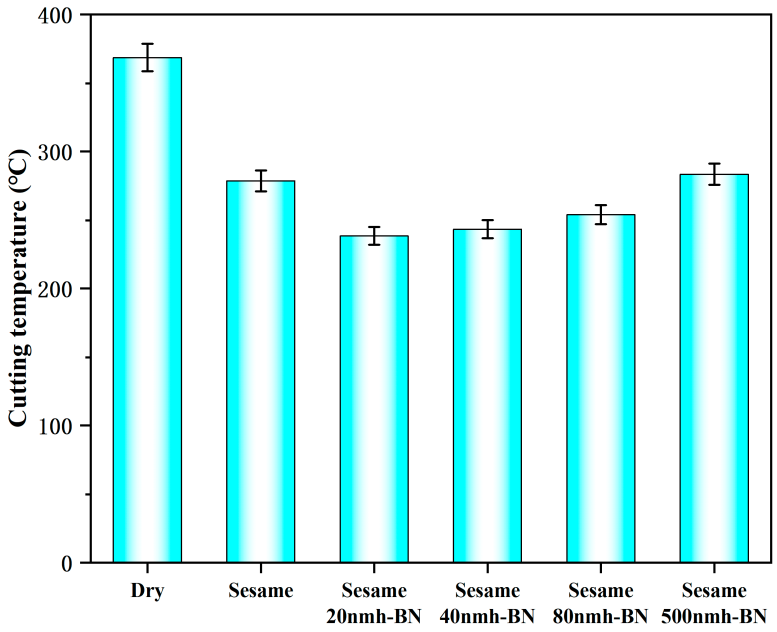


**Figure 14.** Cutting temperature in particle size experiment.

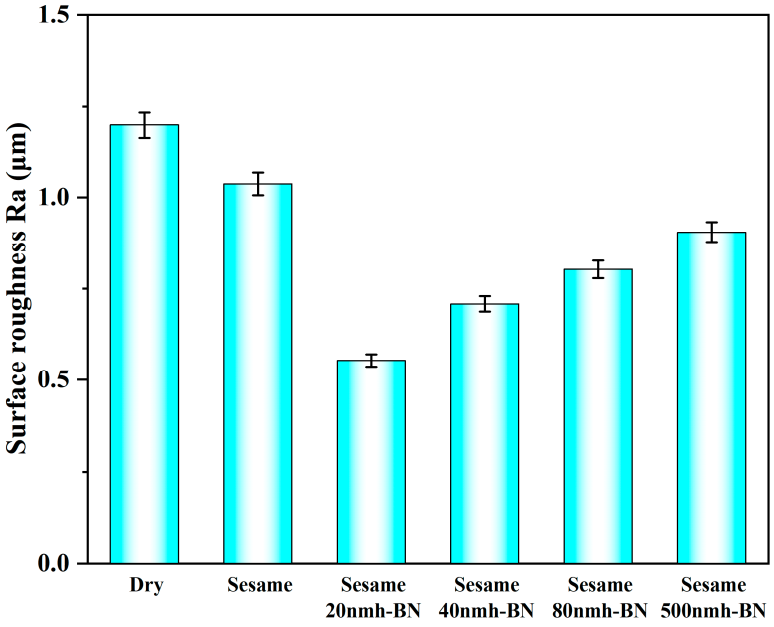


**Figure 15.** Surface roughness of workpiece in different cutting conditions.

Figure 15 shows the surface roughness in different cutting conditions. The rise in cutting temperature has an impact on the surface quality of the workpiece, as evidenced by the workpiece's surface roughness. The findings suggest that when the h-BN particle size in the cutting fluid is at the nanoscale, the surface roughness is better than the surface roughness of dry cutting and pure sesame oil, with a decrease in surface roughness ranging from 46.6% to 53.8%. Additionally, in the case where the h-BN particle size falls within the submicron range, the surface roughness value of the workpiece experiences an increase of 22.7% and 14.6% compared to the Ra values observed during dry cutting and the use of pure sesame oil, respectively. This observation implies that excessively large h-BN particle

sizes not only disturb the protective effect of sesame oil on the machined workpiece surface, but also cause damage to the surface.

### 3.2.3. Microhardness Variation and Work Hardening Capacity

Figure 16 shows the microhardness and work-hardening capacity in different cutting conditions. As shown in Figure 16a, when the h-BN particle size in the cutting fluid is at the nanoscale, there is little difference in the work hardening capacity; compared to the uncut substrate, the microhardness after cutting increases by 15.3% to 20.6%. When the h-BN particle size is in the submicron range, the microhardness after cutting increases by 31.1% compared to the uncut substrate. It has been observed that as the particle size increases, the cutting force, average friction coefficient, and the cutting temperature also increase. This ultimately results in a higher degree of work hardening. As shown in Figure 16b, the trend of the curve is quite similar for all machining conditions. The work-hardened layer reaches a depth of approximately 200–250 μm.

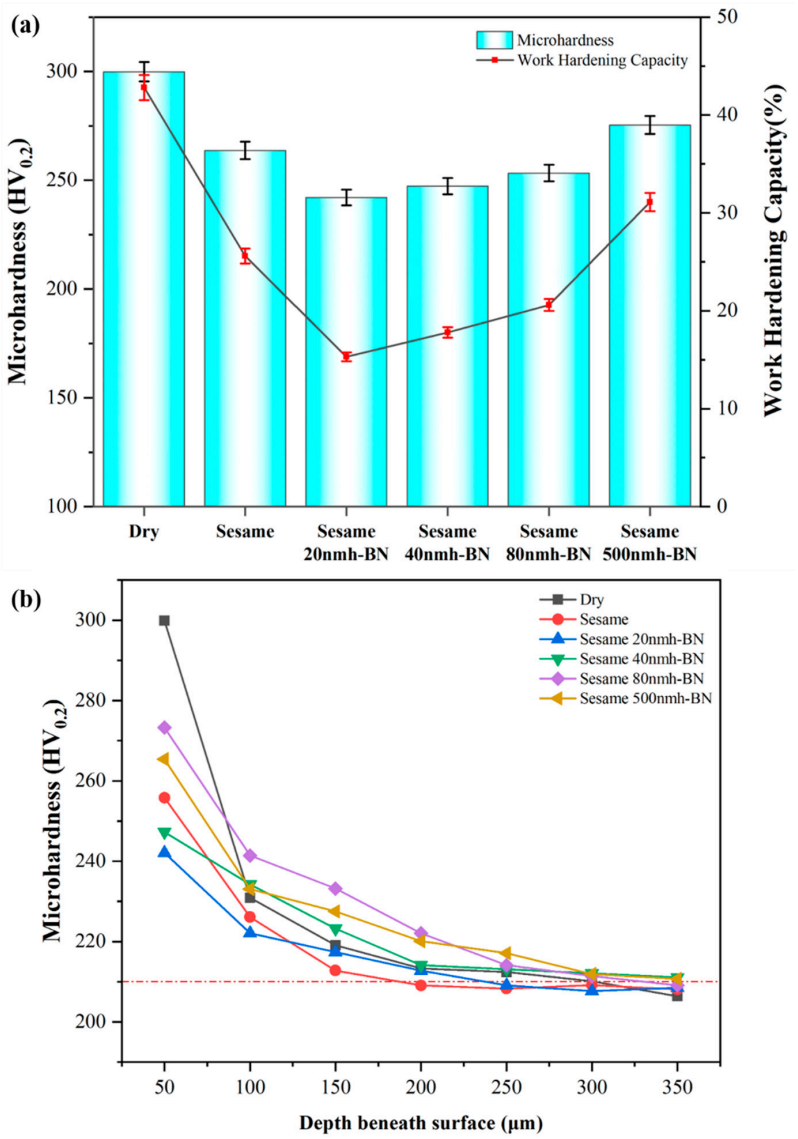


**Figure 16.** Microhardness of machined material and work hardening capacity in different cutting conditions: (**a**) work hardening capacity; (**b**) microhardness of the machined surfaces (the dotted red line represents the microhardness of the substrate).

### 3.2.4. Surface Topography

Figure 17 displays the 3D surface topography and 2D surface profile in different cutting conditions. From Figure 17c–e, it is evident that when a fluid with nanoscale h-BN particles is added, the maximum difference between valleys and peaks is relatively reduced. The 3D surface topography reveals a more balanced distribution of valleys and peaks on the surface. In Figure 17f, it can be observed that when a fluid with submicron-level h-BN particles is added, the richness of valleys and peaks is significantly enhanced compared to the nanoscale particles.

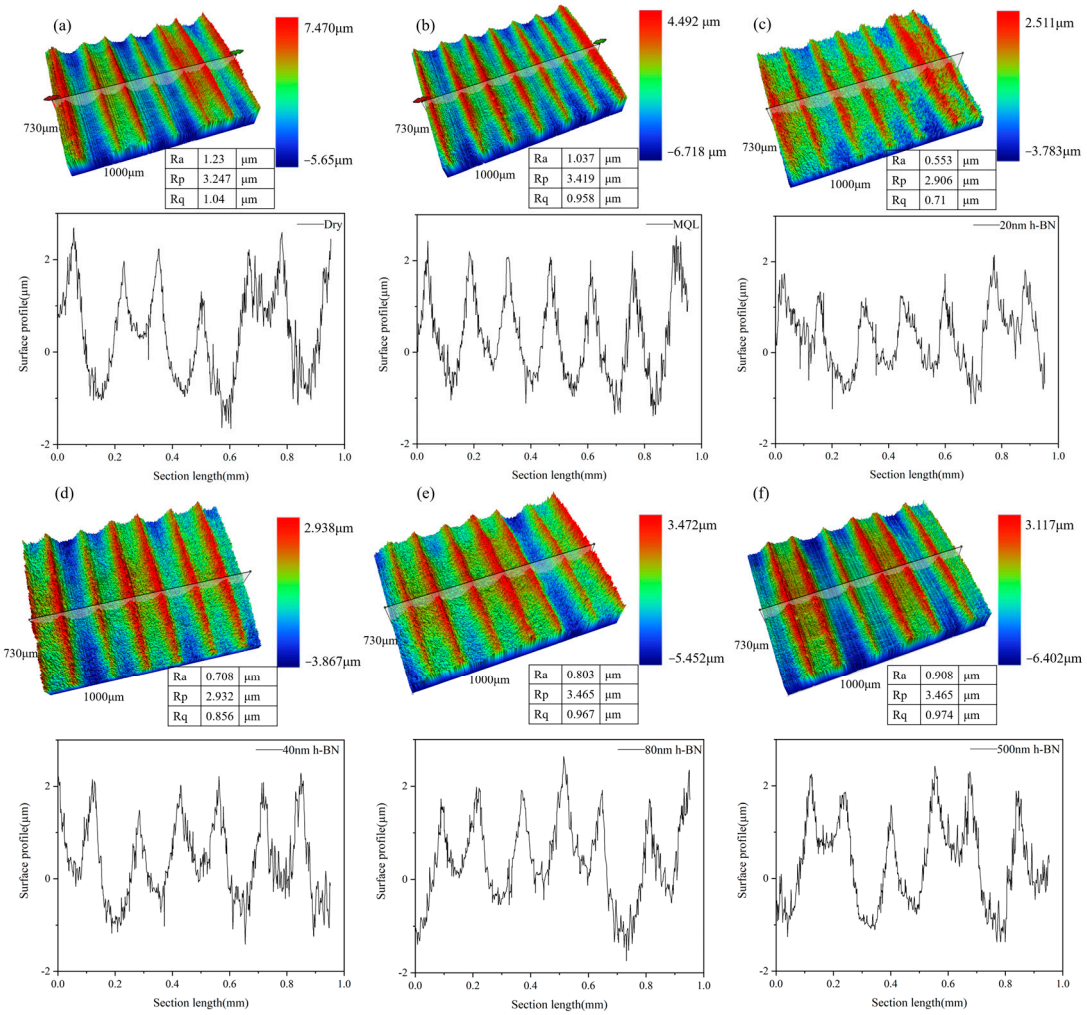


**Figure 17.** The 3D surface topography and 2D surface profile images in different cutting conditions: (**a**) dry, (**b**) sesame oil, (**c**) sesame oil with 20 nm h-BN, (**d**) sesame oil with 40 nm h-BN, (**e**) sesame oil with 80 nm h-BN, and (**f**) sesame oil with 500 nm h-BN.

### 3.2.5. Surface Residual Stress

Figure 18 shows the surface residual stress in different cutting conditions. From Figure 16, it can be observed that the surface residual stress of the sesame oil with nanoscale h-BN particles is smaller than that of sesame oil with submicron-level h-BN particles, and the surface residual stress of the sesame oil with submicron-level h-BN particles is close to that of dry cutting. This is because when nanoscale h-BN particles are added, they have a relatively low rake face friction coefficient, which reduces the effect of frictional forces. This can decrease the surface plastic deformation caused by cutting forces and reduce the generation of residual stress. Additionally, the cutting temperature is relatively low, which is beneficial for reducing thermal stress and residual stress. On the other hand, when submicron-level h-BN particles are added, the larger particles are less likely to enter the

tool–chip contact area and can easily disrupt the lubricating oil film, resulting in higher friction. This increases the cutting forces and cutting temperature, leading to a higher surface residual stress, which does not contribute to enhancing the surface quality of the machined surface.

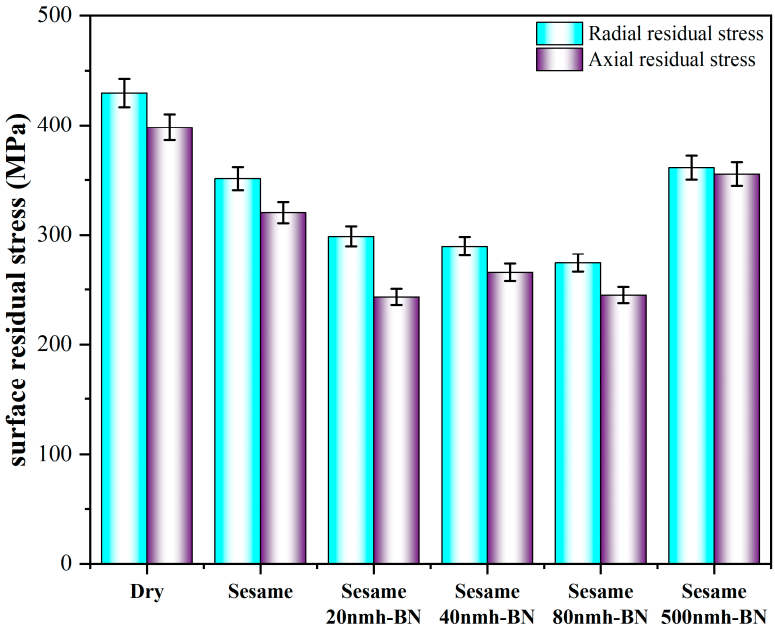


**Figure 18.** Surface residual stress of the workpiece in different cutting conditions.

### 3.2.6. Lubrication Mechanism Analysis

Figure 19 shows the mechanism of nanofluid minimal lubrication. From Figure 19a, it can be seen that there is no lubrication present in dry cutting. From Figure 19b, it can be seen that under MQL, the lubricating oil film provides lubrication and disperses cutting heat, improving the surface quality. From Figure 19c, it can be seen that h-BN nanoparticles exhibit a "polishing effect", micro-polishing the workpiece surface. Additionally, h-BN nanoparticles play a supporting role in the tool–chip contact area, avoiding direct contact between the tool and chips. At the same time, some h-BN nanoparticles also exhibit a "microsphere" effect, transforming sliding friction into rolling friction, thereby reducing the friction between the tool and chips, decreasing the generation of frictional heat, improving the surface quality, and enhancing the integrity of the processed surface.

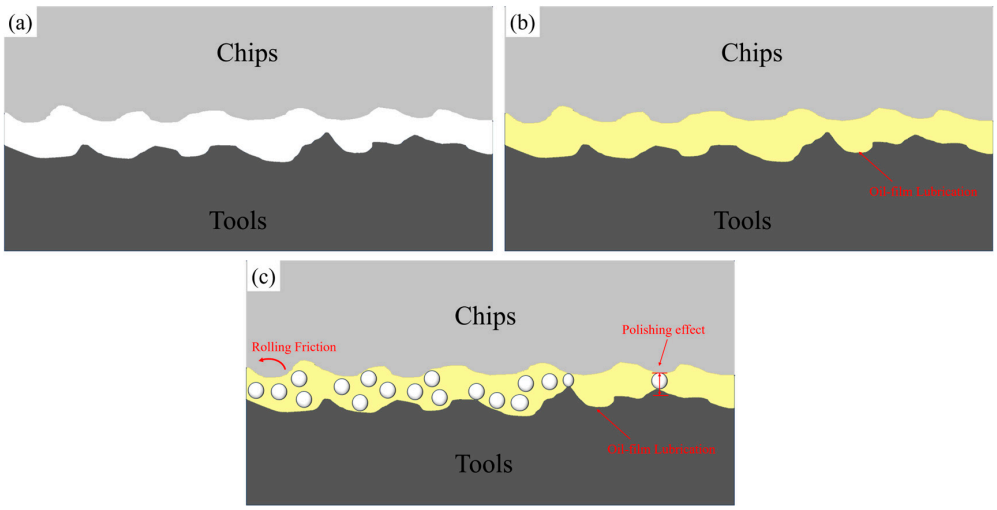


**Figure 19.** Lubrication mechanism: (**a**) dry, (**b**) MQL, (**c**) NMQL.

## 4. Conclusions

This study analyzed the effects of the size and concentration of h-BN nanoparticles added to nanofluids on the surface integrity during the turning process of 304 stainless steel. Based on the conducted research, the main conclusions are as follows:

(1) The utilization of h-BN nanofluid improves the surface quality of the processed surface. The combined lubrication effect of nano-h-BN and sesame oil reduces the average friction coefficient within the tool–chip contact area, thereby effectively reducing the generation of frictional heat. By comparing the addition of 0–5 wt.% h-BN, it was found that adding 3 wt.% h-BN nanofluid resulted in the best surface quality. The cutting temperature, surface roughness, surface residual stress, and work hardening capacity can be reduced by 43.5%, 53.8%, 61.6%, and 27.5%, respectively. The highest friction coefficient can be decreased by 38.9%. The performance is excellent.

(2) By augmenting viscosity and decreasing contact angle, the presence of nanoscale h-BN improves the penetration of the cutting fluid at the interface between the tool and the chip. White-light interferometry results reveal a more balanced distribution of peaks and valleys in the 3D and 2D surface topography. The residual surface stress is lower compared to dry cutting and MQL.

(3) Compared with submicron particles, nanoscale h-BN particles perform better through the tendency of cutting tool and chip interface. Moreover, the h-BN particles in the nanofluid play a "rolling effect" and "microsphere" effect, and the sesame oil will also form a lubricating oil film in the knife–chip contact area, thereby reducing the friction coefficient, reducing the cutting force, and improving the machining surface quality.

The effect of h-BN nanoparticles with different concentrations and particle sizes on the surface integrity shows that it is important to study the concentration and particle size of nanoparticles on the surface integrity of machining. NMQL needs more factors and further analysis. For example, molecular dynamics simulation is introduced to verify the results of cutting experiments, which can be analyzed in future work.

**Author Contributions:** Conceptualization, M.F.; methodology, M.F., H.C. and M.Y.; validation, G.X.; investigation, M.F., G.X. and H.C.; resources, C.X. and G.X.; data curation, M.F. and G.X.; writing—original draft preparation, M.F.; writing—review and editing, M.F., M.Y., J.Z. and Z.C.; supervision, G.X. and C.X.; project administration, G.X. and C.X.; funding acquisition, Z.C. and C.X. All authors have read and agreed to the published version of the manuscript.

**Funding:** This research was funded by the National Natural Science Foundation of China (Grants No. 52075276, No. 52105192), and the Key Research and Development Program of Shandong province (2023CXGC010212).

**Data Availability Statement:** The raw data supporting the conclusions of this article will be made available by the authors on request.

**Conflicts of Interest:** The authors declare no conflict of interest.

## References

1. Sales, W.F.; Schoop, J.; da Silva, L.R.R.; Machado, Á.R.; Jawahir, I.S. A review of surface integrity in machining of hardened steels. *J. Manuf. Process.* **2020**, *58*, 136–162. [CrossRef]
2. Astakhov, V.P. *Tribology of Metal Cutting*; Elsevier: Amsterdam, The Netherlands, 2006.
3. Hussain, G.; Alkahtani, M.; Alsultan, M.; Buhl, J.; Gupta, M.K. Chip formation, cutting temperature and forces measurements in hard turning of Gcr15 under the influence of PcBN chamfering parameters. *Measurement* **2022**, *204*, 112130. [CrossRef]
4. Zhang, W.; Wang, X.; Hu, Y.; Wang, S. Predictive modelling of microstructure changes, micro-hardness and residual stress in machining of 304 austenitic stainless steel. *Int. J. Mach. Tools Manuf.* **2018**, *130–131*, 36–48. [CrossRef]
5. Carvalho, D.O.A.; da Silva, L.R.R.; Sopchenski, L.; Jackson, M.J.; Machado, Á.R. Performance evaluation of vegetable-based cutting fluids in turning of AISI 1050 steel. *Int. J. Adv. Manuf. Technol.* **2019**, *103*, 1603–1619. [CrossRef]
6. Sarıkaya, M.; Şirin, Ş.; Yıldırım, Ç.V.; Kıvak, T.; Gupta, M.K. Performance evaluation of whisker-reinforced ceramic tools under nano-sized solid lubricants assisted MQL turning of Co-based Haynes 25 superalloy. *Ceram. Int.* **2021**, *47*, 15542–15560. [CrossRef]
7. Davim, J.P.; Sreejith, P.S.; Gomes, R.; Peixoto, C. Experimental studies on drilling of aluminium (AA1050) under dry, minimum quantity of lubricant, and flood-lubricated conditions, Proceedings of the Institution of Mechanical Engineers. *Part B J. Eng. Manuf.* **2006**, *220*, 1605–1611. [CrossRef]

8. Sarıkaya, M.; Güllü, A. Multi-response optimization of minimum quantity lubrication parameters using Taguchi-based grey relational analysis in turning of difficult-to-cut alloy Haynes 25. *J. Clean. Prod.* **2015**, *91*, 347–357. [CrossRef]
9. Maruda, R.W.; Arkusz, K.; Szczotkarz, N.; Wojciechowski, S.; Niesłony, P.; Królczyk, G.M. Analysis of size and concentration of nanoparticles contained in cutting fluid during turning of 316L steel in minimum quantity lubrication conditions. *J. Manuf. Process.* **2023**, *87*, 106–122. [CrossRef]
10. Roushan, A.; Rao, U.S.; Patra, K.; Sahoo, P. Performance evaluation of tool coatings and nanofluid MQL on the micro-machinability of Ti-6Al-4V. *J. Manuf. Process.* **2022**, *73*, 595–610. [CrossRef]
11. Sharma, J.; Sidhu, B.S. Investigation of effects of dry and near dry machining on AISI D2 steel using vegetable oil. *J. Clean. Prod.* **2014**, *66*, 619–623. [CrossRef]
12. Tazehkandi, A.H.; Shabgard, M.; Pilehvarian, F. Application of liquid nitrogen and spray mode of biodegradable vegetable cutting fluid with compressed air in order to reduce cutting fluid consumption in turning Inconel 740. *J. Clean. Prod.* **2015**, *108*, 90–103. [CrossRef]
13. Saidur, R.; Leong, K.Y.; Mohammed, H.A. A review on applications and challenges of nanofluids. *Renew. Sustain. Energy Rev.* **2011**, *15*, 1646–1668. [CrossRef]
14. Sharma, A.K.; Tiwari, A.K.; Dixit, A.R. Mechanism of Nanoparticles Functioning and Effects in Machining Processes: A Review. *Mater. Today Proc.* **2015**, *2*, 3539–3544. [CrossRef]
15. Duan, Z.; Li, C.; Zhang, Y.; Dong, L.; Bai, X.; Yang, M.; Jia, D.; Li, R.; Cao, H.; Xu, X. Milling surface roughness for 7050 aluminum alloy cavity influenced by nozzle position of nanofluid minimum quantity lubrication. *Chin. J. Aeronaut.* **2021**, *34*, 33–53. [CrossRef]
16. Shokrani, A.; Betts, J.; Jawahir, I.S. Improved performance and surface integrity in finish machining of Inconel 718 with electrically charged tungsten disulphide MQL. *CIRP Ann.* **2022**, *71*, 109–112. [CrossRef]
17. Makhesana, M.A.; Patel, K.M.; Krolczyk, G.M.; Danish, M.; Singla, A.K.; Khanna, N. Influence of MoS2 and graphite-reinforced nanofluid-MQL on surface roughness, tool wear, cutting temperature and microhardness in machining of Inconel 625. *CIRP J. Manuf. Sci. Technol.* **2023**, *41*, 225–238. [CrossRef]
18. Yıldırım, Ç.V.; Sarıkaya, M.; Kıvak, T.; Şirin, Ş. The effect of addition of hBN nanoparticles to nanofluid-MQL on tool wear patterns, tool life, roughness and temperature in turning of Ni-based Inconel 625. *Tribol. Int.* **2019**, *134*, 443–456. [CrossRef]
19. Wang, Y.; Wan, Z.; Lu, L.; Zhang, Z.; Tang, Y. Friction and wear mechanisms of castor oil with addition of hexagonal boron nitride nanoparticles. *Tribol. Int.* **2018**, *124*, 10–22. [CrossRef]
20. Kim, D.; Lee, P.; Kim, J.; Lee, S. Machinability on micro-end milling process of Ti-6Al-4V with nanofluid minimum quantity lubrication using hexagonal boron nitride particles. In Proceedings of the 4M/ICOMM2015 Conference, Milan, Italy, 31 March–2 April 2015; pp. 158–161.
21. Talib, N.; Rahim, E.A. Performance of modified jatropha oil in combination with hexagonal boron nitride particles as a bio-based lubricant for green machining. *Tribol. Int.* **2018**, *118*, 89–104. [CrossRef]
22. García-Martínez, E.; Miguel, V.; Martínez-Martínez, A.; Coello, J.; Naranjo, J.A.; Manjabacas, M.C. Optimization of the Dry Turning Process of Ti48Al2Cr2Nb Aluminide Based on the Cutting Tool Configuration. *Materials* **2022**, *15*, 1472. [CrossRef]
23. Zhang, Y.; Li, C.; Jia, D.; Zhang, D.; Zhang, X. Experimental evaluation of MoS2 nanoparticles in jet MQL grinding with different types of vegetable oil as base oil. *J. Clean. Prod.* **2015**, *87*, 930–940. [CrossRef]
24. Gao, T.; Zhang, X.; Li, C.; Zhang, Y.; Yang, M.; Jia, D.; Ji, H.; Zhao, Y.; Li, R.; Yao, P.; et al. Surface morphology evaluation of multi-angle 2D ultrasonic vibration integrated with nanofluid minimum quantity lubrication grinding. *J. Manuf. Process.* **2020**, *51*, 44–61. [CrossRef]
25. Jianxin, D.; Ze, W.; Yunsong, L.; Ting, Q.; Jie, C. Performance of carbide tools with textured rake-face filled with solid lubricants in dry cutting processes. *Int. J. Refract. Met. Hard Mater.* **2012**, *30*, 164–172. [CrossRef]
26. Goyal, A.; Kothari, B.; Pathak, V.K. Fuzzy logic and desirability based models for predicting performance characteristics of varying concentration graphite nanoplatelets (GNPs) mixed nanofluid MQL in turning of AISI-1045 steel. *Int. J. Interact. Des. Manuf. (IJIDeM)* **2022**, *16*, 1559–1584. [CrossRef]
27. Sen, B.; Mia, M.; Gupta, M.K.; Rahman, M.A.; Mandal, U.K.; Mondal, S.P. Influence of Al2O3 and palm oil–mixed nano-fluid on machining performances of Inconel-690: IF-THEN rules–based FIS model in eco-benign milling. *Int. J. Adv. Manuf. Technol.* **2019**, *103*, 3389–3403. [CrossRef]
28. Singh, R.; Sharma, V. Experimental investigations into sustainable machining of Hastelloy C-276 under different lubricating strategies. *J. Manuf. Process.* **2022**, *75*, 138–153. [CrossRef]
29. Gupta, M.K.; Song, Q.; Liu, Z.; Sarikaya, M.; Jamil, M.; Mia, M.; Singla, A.K.; Khan, A.M.; Khanna, N.; Pimenov, D.Y. Environment and economic burden of sustainable cooling/lubrication methods in machining of Inconel-800. *J. Clean. Prod.* **2021**, *287*. [CrossRef]
30. Habibnia, M.; Sheikholeslami, M.; Tabarhoseini, S.M.; Taheri, A.; Sheykhi, M. Cooling improvement for the machining process with the inclusion of nanoparticles using the experimental approach. *J. Mol. Liq.* **2023**, *370*, 120985. [CrossRef]
31. Sartori, S.; Ghiotti, A.; Bruschi, S. Solid Lubricant-assisted Minimum Quantity Lubrication and Cooling strategies to improve Ti6Al4V machinability in finishing turning. *Tribol. Int.* **2018**, *118*, 287–294. [CrossRef]

32. Hadad, M.; Hadi, M. An investigation on surface grinding of hardened stainless steel S34700 and aluminum alloy AA6061 using minimum quantity of lubrication (MQL) technique. *Int. J. Adv. Manuf. Technol.* **2013**, *68*, 2145–2158. [CrossRef]
33. Zhuang, K.; Zhou, S.; Zou, L.; Lin, L.; Liu, Y.; Weng, J.; Gao, J. Numerical investigation of sequential cuts residual stress considering tool edge radius in machining of AISI 304 stainless steel. *Simul. Model. Pract. Theory* **2022**, *118*, 102525. [CrossRef]